PROCEEDINGS OF SCIENCE

Optical Potential Analysis of Antiproton-Nucleus Data at Low Energy

A. Bianconi,[a,b] **V. Mascagna,**[a,b] **S. Migliorati**[a,b,*] **and L. Venturelli**[a,b]

[a] *Dipartimento di Ingegneria dell'Informazione, Università degli Studi di Brescia, via Branze 38, Brescia, Italy*

[b] *INFN Pavia, via Agostino Bassi, Pavia, Italy*

E-mail: luca.venturelli@unibs.it

The study of antiproton-nucleus interactions at low and very low energies is important for understanding nuclear dynamics and interactions. In this work, we analyze antiproton elastic scattering and annihilation cross-section data using an optical model approach. By employing the Woods-Saxon potential, we extract meaningful parameters to describe the interaction and provide insight into momentum dependence. The results indicate good agreement with experimental data, while also suggesting hidden dependencies on momentum in potential parameters. Future improvements involve refining computational techniques and exploring alternative parameterizations to achieve more precise modeling.

EXA/LEAP2024,
26-30 August 2024
Austrian Academy of Sciences, Vienna, Austria

[*] Speaker

1. Introduction

Antiproton interactions with nuclei provide valuable insight into nuclear structure and strong force dynamics. Experimental data from LEAR (1980s-1990s) [1–4] and AD (2000s-present) [5–7] have enabled precise measurements of antiproton elastic scattering and annihilation cross-sections. However, the study of low-energy antiproton interactions (p < 300 MeV/c) remains incomplete, particularly at very low energies (p < 100 MeV/c). This work aims to analyze such interactions using an optical potential model, focusing on momentum dependence and model validation.

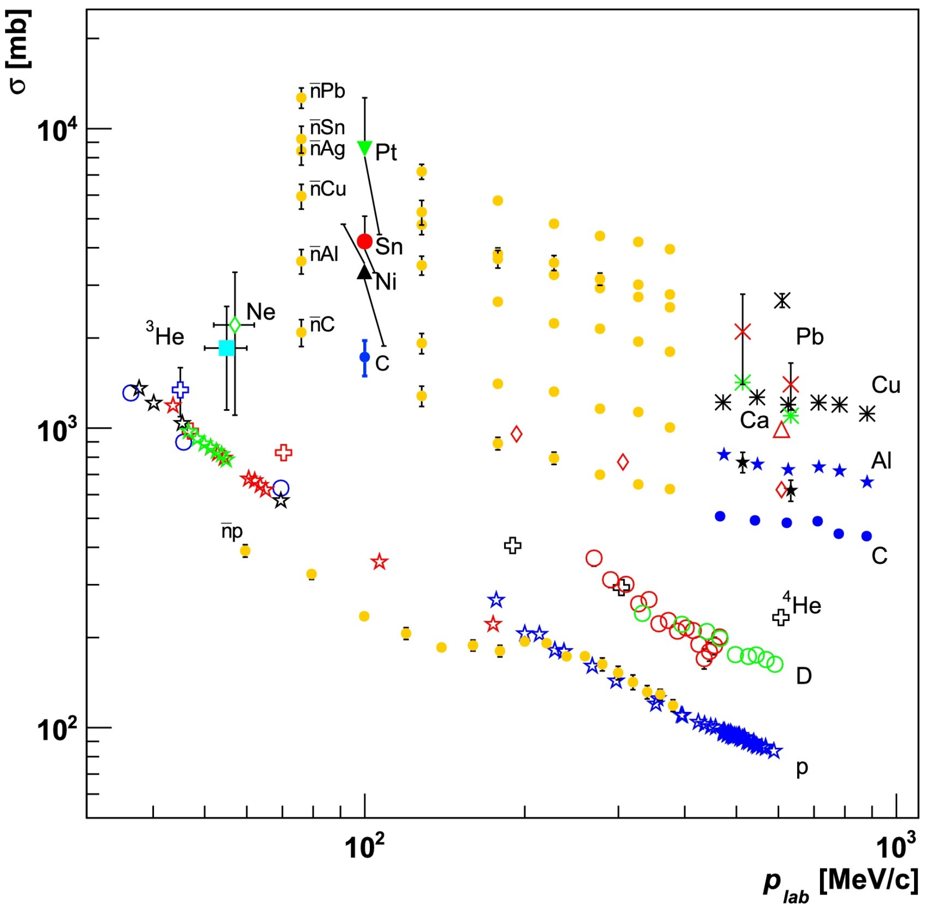

Figure 1: Antinucleon annihilation cross-section measurements for kinetic energies below 500 MeV (from Ref. [6], where details and references are available). Antineutron data (*ochre*) are from the OBELIX experiment at CERN. Antiproton data symbols: ☆ for H (from OBELIX and PS173 experiments at CERN), ○ for D (from OBELIX, Kalogeropoulos et al. at BNL, and Bizzarri et al. at CERN), × for ^{4}He (from OBELIX and the PS179 experiment at CERN), ■ for ^{3}He (from OBELIX), • for C (from the ASACUSA experiment at CERN and from Nakamura et al. at KEK), ◇ for Ne (from PS179), ★ for Al (from Nakamura et al. and Ashford et al. at AGS), △ for Ca (from Garreta et al. at CERN), ✳ for Cu (from Nakamura et al. and Ashford et al.), × for Pb (from Ashford et al. and Garreta et al.), ▲ for Ni, • for Sn, and ▼ for Pt (from ASACUSA).

2. Data and Methodology

The analysis begins by considering scattering data from LEAR experiments for different nuclei at various momenta, as listed in Table 1. These data were extracted from published plots, as they are not available in online databases.

Nucleus	Momentum (MeV/c)	Angle Range (deg)	Measured Points
^{12}C	300/608	5-65	44/46 [8–10]
^{16}O	605.5	5-65	29 [10]
^{40}Ca	303/608	5-45/5-55	23/43 [8–10]
^{208}Pb	305/609	5-40/5-45	19/40 [8–10]

Table 1: Sets of elastic scattering data, see the cited references for the values.

We model the nuclear interaction using a Woods-Saxon potential [11] (Eq. (1)) and solve the non-relativistic Schrödinger equation numerically within a partial-wave formalism:

$$U_{WS}(r) = V_0 f(r, r_{0R}, a_R) + iW_0 f(r, r_{0I}, a_I) \tag{1}$$

where

$$f(r, r_{0x}, a_x) = \left[1 + \exp\left(\frac{r - r_{0x}A^{1/3}}{a_x}\right)\right]^{-1}$$

The parameters are: V_0 and W_0 (depths of the real and imaginary potentials), r_{0R} and r_{0I} (radius parameters for the real and imaginary potentials), a_R and a_I (diffuseness parameters for the real and imaginary potentials), and A (mass number of the nucleus). The variable r is the radial distance from the center of the nucleus. The function $f(r, r_{0x}, a_x)$ describes a Fermi-type distribution, ensuring a smooth transition of the potential from the central region to the exterior.

The solutions give the scattering amplitude A_S, which contains the information about the nucleus and the interaction with the projectile with wave number $k = p/\hbar$, from which the differential elastic cross-section can be evaluated.

$$\frac{d\sigma_{\text{el}}}{d\Omega} = |A_S(\theta, k)|^2 \tag{2}$$

We fitted the calculated cross-sections to existing data to determine the model parameters and validate the model through the minimization of the following χ^2 function, which incorporates a pull term λ for normalization.

$$\chi^2 = \min_{\lambda}\left[\sum_i^N \left(\frac{\sigma^{ex}(x_i) - \lambda\sigma^{th}(x_i)}{\Delta\sigma_i}\right)^2 + \left(\frac{\lambda - \lambda_0}{\Delta\lambda}\right)^2\right]$$

The number of free parameters varies from 5 to 7. The potential depths (V_0 and W_0) are always free parameters. The geometrical parameters (a_R, a_I, r_{0R}, r_{0I}) can be different between the real and imaginary part or can be set equal in pairs ($a_R = a_I$ and/or $r_{0R} = r_{0I}$).

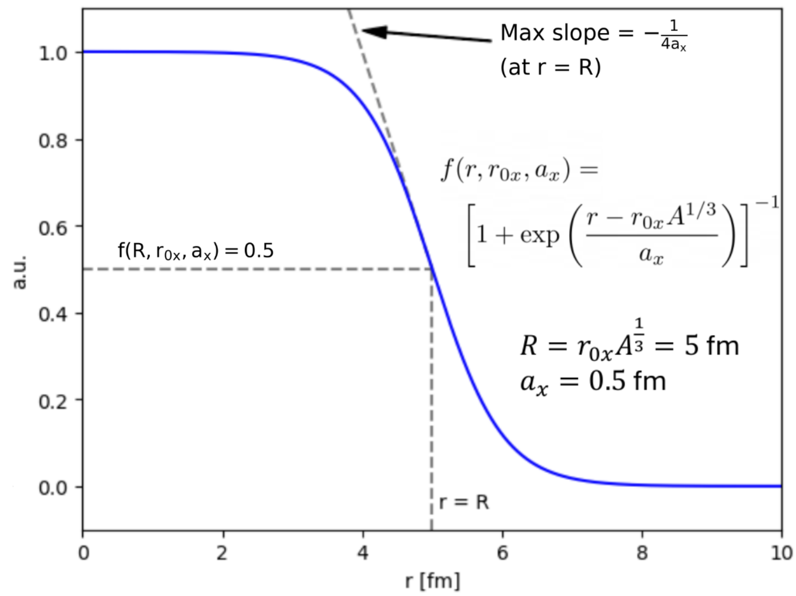

Figure 2: Woods-Saxon potential [11] (Eq. (1)).

3. Results and Discussion

The analysis was initially conducted using the elastic cross sections. Here we discuss only the case of the ^{12}C target using datasets at 300 MeV/c and 608 MeV/c (see Fig. 3). The obtained parameters are reported in Table 2.

p [MeV]	n_{par}	U_0 [MeV]	W_0 [MeV]	r_{0R} [fm]	r_{0I} [fm]	a_R [fm]	a_I [fm]	λ	$\tilde{\chi}^2$
300	5	18 ± 5	27 ± 12	1.35 ± 0.13	—	0.43 ± 0.07	—	1.19 ± 0.03	0.78
	6	23 ± 5	16 ± 6	1.3 ± 0.1	1.5 ± 0.1	0.40 ± 0.05	—	1.0 ± 0.1	0.70
	7	23 ± 5	16 ± 5	1.3 ± 0.1	1.5 ± 0.1	0.4 ± 0.1	0.4 ± 0.1	1.00 ± 0.09	0.72
608	5	71 ± 7	159 ± 18	0.97 ± 0.03	—	0.478 ± 0.009	—	1.20 ± 0.03	0.90
	6	52 ± 15	179 ± 29	1.05 ± 0.08	0.94 ± 0.04	0.477 ± 0.009	—	1.22 ± 0.03	0.92
	7	64 ± 20	158 ± 44	1.03 ± 0.08	0.96 ± 0.06	0.43 ± 0.06	0.49 ± 0.02	1.21 ± 0.04	0.93

Table 2: Best-fit parameters for ^{12}C target. The empty cells are for geometrical parameters which were forced to be the equal to the corresponding real part values.

Good agreement has been obtained between the model and the experimental data, as also visible in Fig. 3 for the ^{12}C data at 608 MeV/c. However, changing the momentum the values of the parameters – in particular the potential depths – seems to change considerably. This could be a clue to some parameters' hidden dependence on momentum, a possibility explored in other potential models [12].

The same parameters obtained from the fit were used to calculate the annihilation cross sections, which were then compared with the experimental annihilation data reported in Table 3.

Nucleus	Momentum(MeV/c)	Measured points
^{12}C	100-900	7 [6]
^{40}Ca	610	1 [8, 9]
^{208}Pb	500-650	3 [6]

Table 3: Datasets of the antiproton annihilation cross sections.

The results are plotted in Fig. 4. The dependence on momentum is also evident in this case, as using parameters from a different dataset—i.e., with a different momentum—better reproduces the annihilation data near that momentum compared to others.

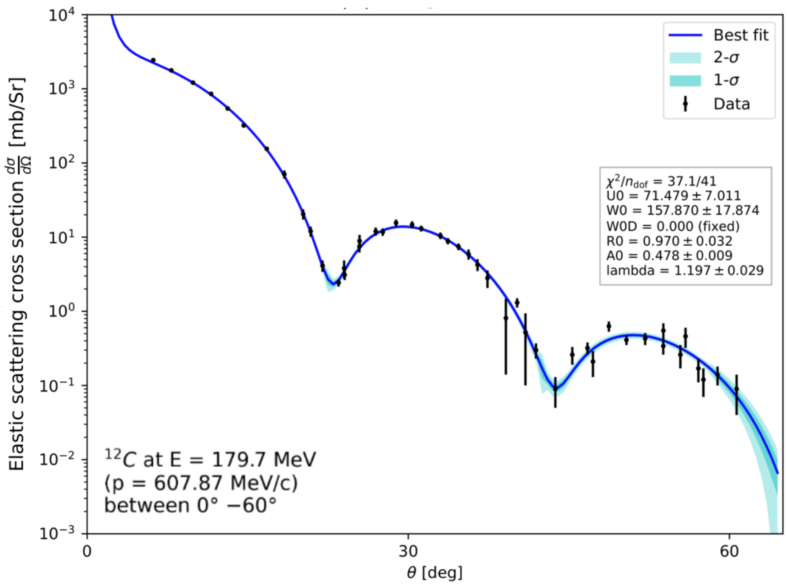

Figure 3: Experimental data for ^{12}C at E = 179.7 MeV (p = 607.87 MeV/c) between $0° - 60°$ with the best-fit curve and error bands at 1σ and 2σ.

The elastic scattering differential cross sections have also been computed for momenta lower than those in the available datasets. These projections help assess the feasibility and limitations of future experiments on nuclear scattering. For all the considered targets, distinguishing nuclear elastic scattering effects from Coulomb interactions becomes experimentally challenging below 50 MeV/c. Therefore, future experiments should prioritize momenta above 50 MeV/c for nuclear interaction studies.

4. Future Developments

To enhance the accuracy and applicability of our model, we propose:

1. Improving computational efficiency and precision in parameter fitting. (The fitting procedure occasionally fails to converge. Possible causes include an unsuitable model for the data, high correlation between parameters, an inadequate choice of initial parameter values).

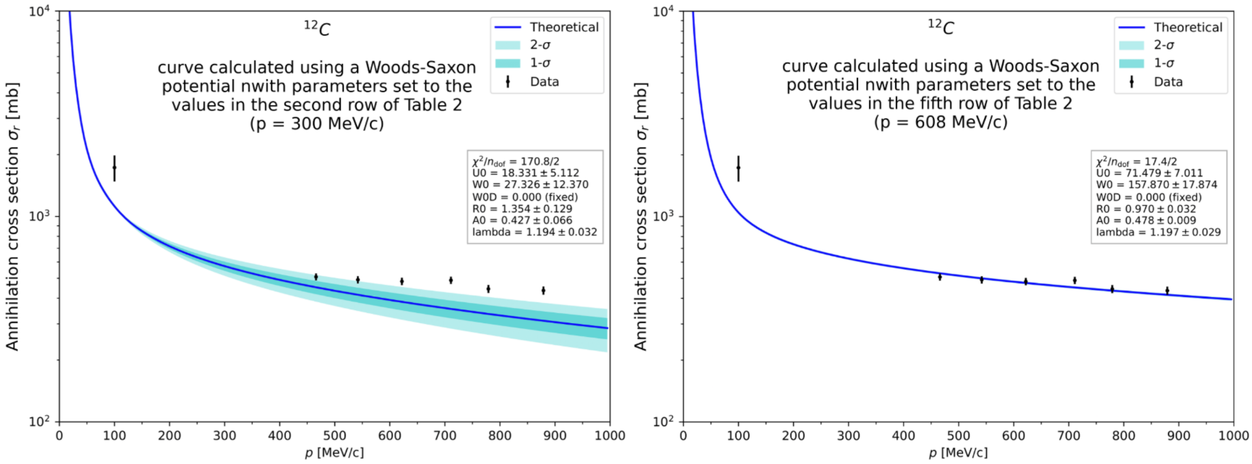

Figure 4: Antiproton annihilation cross-section data with curves calculated using the best-fit results from the analysis of elastic data at 300 MeV/c (left) and 607.9 MeV/c (right).

2. Exploring alternative parameterizations, such as:
   - Scattering length approach [13].
   - Momentum-dependent potentials [12].
3. Implementing a global fitting strategy that optimally combines elastic and annihilation cross-sections via χ^2 minimization.

5. Conclusion

This work presents an optical potential analysis of low-energy antiproton-nucleus interactions using data from LEAR and AD experiments. Our results show good agreement with experimental observations while indicating significant momentum dependence in the derived potential parameters. Future studies should focus on refining theoretical models and conducting additional experiments at suitable momentum ranges to enhance our understanding of nuclear interactions.

References

[1] C. Amsler and F. Myhrer, *Low Energy Antiproton Physics*, *Annu. Rev. Nucl. Part. Sci.* **41** (1991) 219-267.

[2] G. Bendiscioli and D. Kharzeev, *Antinucleon-nucleon and antinucleon-nucleus interactions*, *La Rivista del Nuovo Cimento* **17** (1994) 1-65.

[3] A. Donnachie, *Low-energy hadronic physics*, *Physics Reports* **403–404** (2004) 281–301.

[4] C. Amsler, *Nucleon-antinucleon annihilation at LEAR*, *ArXiv:1908.08455 [hep-ph]*, 2019.

[5] A. Bianconi et al., *Measurement of the antiproton–nucleus annihilation cross section at 5.3 MeV*, *Phys. Lett. B* **704** (2011) 461-466.

[6] H. Aghai-Khozani et al., *Measurement of the antiproton–nucleus annihilation cross-section at low energy*, *Nucl. Phys. A* **970** (2018) 366.

[7] H. Aghai-Khozani et al., *Limits on the antiproton-nuclei annihilation cross sections at 125 keV*, *Nucl. Phys. A* **1009** (2021) 122170.

[8] D. Garreta et al., *Elastic scattering of antiprotons from carbon, calcium, and lead at 180 MeV*, *Phys. Lett. B* **149** (1984) 64-68.

[9] D. Garreta et al., *Scattering of antiprotons from carbon at 46.8 MeV*, *Phys. Lett. B* **135** (1984) 266-270.

[10] S. Janouin et al., *Optical-model analysis of antiproton-nucleus elastic scattering at 50 and 180 MeV*, *Nucl. Phys. A* **451** (1986) 541-561.

[11] P. E. Hodgson, *The nuclear optical model*, *Rep. Prog. Phys.* **34** (1971) 765-819.

[12] T.-G. Lee and C.-Y. Wong, *Momentum-dependent optical potentials for antiprotons*, *Phys. Rev. C* **97** (2018) 054617.

[13] C. Batty et al., *Antiprotonic atom data and analysis*, *Nucl. Phys. A* **689** (2001) 721-740.